The CEBAF Injection Line as One Big Stern-Gerlach Polarimeter

Richard Talman, Laboratory of Elementary-Particle Physics, Cornell University;
Joe Grames, Reza Kazimi, Matt Poelker, Riad Suleiman, Thomas Jefferson National Laboratory;
Brock Roberts, University of New Mexico

22nd International Spin Symposium
University of Illinois and Indiana University
Urbana-Champaign, 2016

September 6, 2016 draft

ABSTRACT. It is explained how the CEBAF 123 MeV injection line can be instrumented to serve as one big Stern-Gerlach polarimeter measuring the polarization state of the injected beam. No physical changes to the line are required but resonant beam position monitors, much like others already present in the ring, need to be judiciously located at locations favorable for detecting the Stern-Gerlach signal.

The historical Stern-Gerlach apparatus used a uniform magnetic field (to orient the spins) with quadrupole magnetic field superimposed (to deflect opposite spins oppositely) and a neutral, somewhat mono-energetic, unpolarized, atomic beam. For the highly-monochromatic, already-polarized beam produced by an electron gun, the uniform magnetic field has become superfluous, and every quadrupole in the injection line produces polarization-dependent Stern-Gerlach deflection.

Dual CEBAF electron beam guns produce superimposed 0.25 GHz (bunch separation 4 ns) electron beams for which the polarization states and the bunch phases can be adjusted individually. For example, the (linear) polarizations can be opposite and the bunch phases adjusted so that (once superimposed) the bunch spacings are 2 ns and the bunch polarizations alternate between plus and minus. The effect of this beam preparation is to produce a bunch repetition frequency of 0.5 GHz different from the bunch polarization frequency of 0.25 GHz. This difference will make it possible to distinguish Stern-Gerlach-induced bunch deflections from charge-induced deflections.

Transverse bunch displacements can be measured using resonant beam position monitors (BPMs). In particular a high-Q, TM_{210} mode, rectangular cavity, tuned to a particular frequency f_r rings up to a level proportional to the f_r Fourier frequency component of transverse beam displacement. Because linac bunches are short there can be significant resonator response at any one of the strong low order harmonics of the 0.25 GHz bunch polarization frequency.

Our proposed BPMs are tuned to $f_r = 0.75$ GHz. This is the 3th harmonic of the bunch polarization frequency, but not a harmonic of the 0.5 GHz bunch charge frequency. This greatly enhances the sensitivity to transverse bunch displacement correlated with bunch polarization relative to bunch displacement correlated with bunch charge.

This paper estimates the beam quality and the BPM quality required to extract beam polarizations from multiple BPMs along the CEBAF 123 Mev electron injection line. This is expected to provide a passive (non-destructive) form of high analyzing power polarimetry.

Contents

1. Qualitative Discussion of Resonant Stern-Gerlach Detection

It is shown in a later section that Stern-Gerlach (S-G) angular deflections in a few quadrupoles at the upstream end of the CEBAF 123 MeV injection line cause betatron excursions of order one Å(10^{-10} m) downstream. This betatron excitation occurs automatically, with no new active apparatus required. However, to detect these oscillations, special resonant beam position monitors (BPMs) have to be optimally placed at locations where the S-G amplitudes are large. If currently available (not terribly high Q-value) BPMs could be tuned to the required S-G frequency (tentatively taken here to be 0.75 GHz) they would probably be satisfactory. However, sophisticated, special purpose, external data processing electronics will need to be developed.

As a proof of principle for S-G polarimetry, this paper discusses the feasibility of detecting these S-G-induced betatron oscillations using resonant, room temperature copper, BPMs. (For higher selectivity, superconducting BPMs would be superior.)

Recent development of BPMs for precision beam position determination has been motivated by International Linear Collider (ILC) requirements[**1**][**2**][**3**]. This is because the beam positions at the collision points need to be controlled to a precision of roughly 10 Å. Roughly speaking, the ILC BPM prototypes have achieved transverse position reproducibility of ±15 nm, for bunch to bunch variation of beam bunches containing $N_e = 10^{10}$ electrons. This is roughly an order of magnitude greater than (i.e. inferior to) their theoretical-minimum expected resolution of ±1.8 nm. The authors (persuasively) ascribe the performance short-fall primarily to error sources other than thermal noise, such as instrument imperfections or cross-talk from spurious, forbidden-mode response to bunch charge.

These ILC-motivated BPM performance investigations are quite relevant to our proposed Stern-Gerlach (S-G) detection experiment. But it is also important to identify differences that will make it possible to make up the seemingly two order of magnitude improved precision needed for confident S-G effect detection. To mangle a familiar simile, comparing the two experiments is like comparing the presence of apples with the absence of oranges (as will be explained next.)

Resonant beam position detection relies on two TM cavities. One is tuned to a waveguide mode approriate for bunch charge measurement; the other is tuned to a mode sensitive to transverse beam position. Typically both cavities have the same dimensions and shape, either rectangular of cylindrical, but tuned to a symmetric mode for charge detection and an anti-symmetric mode for position detection. ILC tests have typically employed cylindrical TM_{010} mode for charge, TM_{110} mode for position, with mode degeneracy broken by output coupling. For simplicity in avoiding mode degeneracy, the present paper assumes rectangular cavity shape. Figure 1 shows the TM_{210} mode position-sensitive cavity. With width a reduced by a factor of two, a TM_{110} mode cavity could be used for beam charge normalization. The performance of circular and rectangular BPMs is expected to be similar.

(By the Heisenberg uncertainty principle) it would not be feasible to locate a single mono-energy electron with usefully small transverse accuracy. This makes the electron charge e unnaturally small for present purposes. For comparison we define a "standard macrocharge" as the charge of $N_e = 10^{10}$ electrons, which is a typical number of

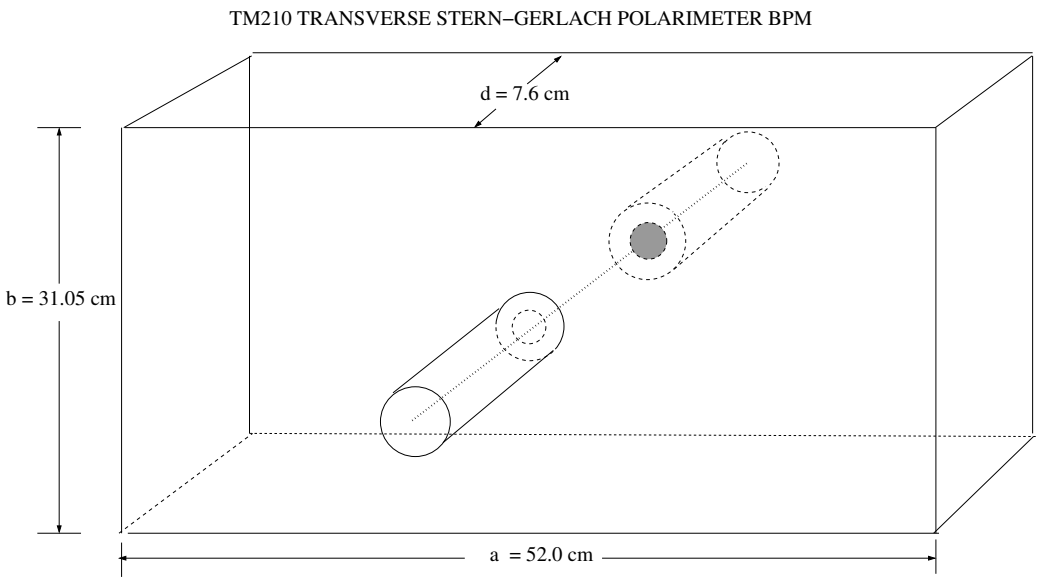

FIGURE 1. Rectangular TM_{210} mode beam position monitor. The cavity dimensions have been roughly adjusted to investigate the performance of the CEBAF 143 MeV injection line as one big Stern-Gerlach polarimeter. Low order TM mode frequencies in GHz are: (1,1,0)= 0.56227, (2,2,0)=1.1245, (1,2,0)=1.0076, (2,1,0)=0.7519. See Figure 5. All modes have $Q = 29338$. For TM_{210} the half-power frequency points (assuming room temperature copper construction) are $0.7519\,\text{GHz} \pm 25.6\,\text{kHz}$.

electrons in each bunch in an ILC prototype test. Classical (rather than quantum) mechanics is adequate for treating the centroid motion of such a large number of electrons, even as regards their mean spin orientation.

A CEBAF beam is CW, with beam current of, say, $160\,\mu$A, which corresponds to a current of about 10^5 macrocharges per second. For S-G detection, as introduced already, the Ångstrom is a natural transverse length unit. For successful ILC operation the transverse beam positions need to be controlled to about 1 nm; i.e. ± 10 Å.

The bunch structures of the CEBAF injector (123 MeV, $160\,\mu$A, 0.5 GHz) and the Accelerator Test Facility (ATF) at the KEK laboratory (1.3 Gev, $N_e e = 10^{10} e$ macrocharge at 5 Hz pulse rate) are very different. We ignore the energy difference, which is thought to be unimportant for the comparison. For a typical cavity resonator quality factor of $Q_r = 10^4$ and frequency of 1 GHz, the cavity charging time is about $10\,\mu$s, which is far shorter than the ATF repetition period. This makes it appropriate to treat the ATF resonant response on a pulse-by-pulse basis. The previously-introduced ± 10 Å r.m.s. transverse position tolerance refers to individual bunch centroids variation. Essentially different in time structure, the CEBAF resonator response is continuous wave (CW) with the previously-defined macrocharges passing through the cavity at 100 kHz rate.

For the narrow band signals under discussion the random noise to signal ratio can be expected to fall proportional to the square root of data collection time. This suggests

that, to the extent spatial imprecision is dominated by thermal noise, two orders of magnitude improved precision will already be made up in runs of one second duration. *There are various reasons why this estimate is irrelevant, or at least misleading.* First of all, it was already stated that the ILC R&D test imprecision is dominated by effects other than random noise in the BPMs. The "good news" to be drawn from this is that random noise is even less limiting for S-G detection than the previous estimate suggested. The "bad news" is that there is little reason to suppose that S-G detection confidence can be improved appreciably by increasing data collection times. (This comment will need to be retracted later, while discussing synchronous detection.) Re-expressed in different terms, the problem limiting S-G detection is not likely to be "too-small amplitude BPM signal"; the problem can be expected to be "too-great spurious background signals mimicking S-G induced transverse betatron excursions".

For better understanding of this comment it is important to understand the essential difference between the two experiments being compared. Using a TM_{210} mode BPM to control the transverse ATF beam position is a null experiment. (Here, and from now on, to avoid switching between waveguide mode notations, we pretend all resonators are rectangular, even when describing experiments that actually used cylindrical resonators.) In the absence of error sources, the transverse BPMs would all read zero for the passage of every macrocharge. Non-zero readings due to spurious background excitations can only be interpreted as being due to the transverse displacements of successive bunches from their design positions. From previously-determined calibrations, non-zero signal amplitude standard deviations are translated into transverse displacement standard deviations.

The statistical issues for S-G-induced betatron detection are very different. Beam current, beam polarization, and lattice parameters such as quadrupole strengths and locations are all known in advance to excellent accuracy. From the unambiguous, non-controversial, Stern-Gerlach theory, this makes it possible to dead-reckon the expected S-G-induced betatron orbits to amply high accuracy. One knows, therefore, *exactly* what one is measuring when one seeks to demonstate the Stern-Gerlach effect in the proposed experiment. Ideal transverse BPMs would read exactly the predicted betatron displacements.

Two BPM attributes are *not known* however. One of these things is whether, in the absence of all imperfections, the BPM sensitivity is good enough to detect the theoretically-knowm S-G deflections. Implications of the preceeding discussion of ILC prototype tests indicate that the BPM sensitivity can be expected to be good enough for S-G detection. This claim will be justified more quantitatively below.

The difficulting of detecting an S-G-induced betatron oscillation of $10^{-11}\,\mathrm{m}$ can be compared to detecting a gravity-wave-induced positional oscillation of $10^{-18}\,\mathrm{m}$ in the LIGO experiment. Like the LIGO experiment statistically-decisive conclusions can be drawn by comparing the responses of more than one, otherwise-statistically-independent detector. The gravitational wave detection has the advantage that the statistical independence of their detectors is more persuasive. But the S-G detection can use more detectors, both horizontal and vertical.

The gravity wave detectibility was enhanced by the availability of templates (unique for given source mechanism, but typically with more that two parameters for fitting) for various possible gravitational wave sources. Of these, in their recent results, the template for a black hole binary collision matched an observed signal coincidence between the two detectors. There is a zero parameter "template" for S-G detection. It is derived in a later section of this paper. Furthermore, unlike the black hole template, which is restricted to less than 100 cycles lasting for as much as a second, the S-G template applies for billions of cycles, lasting over minutes.

A further advantage for S-G detection is the possibility of phase-locked detection, since the frequency and phase of the drive signal are under external control. With the possible modulation of the beam polarizations there is further frequency domain separation of the foreground polarization signal from spurious beam charge induced background signals. For all of these reasons the "smallness" of the S-G signal relative to detection sensitivity is not a fundamental problem.

What can, however, limit the S-G detectibility is the "largeness" of the background/foreground ratio. The only significant fundamental background signals limiting Stern-Gerlach detection come from mechanisms for which the electron beam charge passing through the beam position monitors produces spurious signals that mimic the effect of the beam polarization. Some of the S-G background rejection features mentioned so far may not reduce these background signals.

The main rejection of spurious signals caused by beam charge will be the beam preparation that separates the S-G frequency from the beam charge frequency. Further background rejection will come polarization modulation and from the predicted dependence of S-G signal on BPM location. One expects this dependence to be uncorrelated with the spurious signal background dependence on BPM location.

An eventual purpose for Stern-Gerlach polarimetry will be for the control of frozen spin beams in storage rings. Unlike the case that has been discussed, in this case each particle passes through each BPM millions of times. Noise and background issues in this case will be very different.

2. Stern-Gerlach Detection Enhancement by Background Rejection

Only a single impediment to S-G detection therefore remains. The response to passing charge of a perfectly constructed and aligned TM_{210}, sufficiently narrow band, position sensitive cavity can, theoretically, be insensitive to the beam charge. But, realistically, the cavity response can be dominated by sensitivity to charge, irrespective of transverse beam displacement.

2.1. Background Rejection by Beam Centering. We have seen already that the measured ATF transverse position resolution of $\pm 15\,\mathrm{AA}$ is dominated by spurious responses to beam charge, in conjunction with various other imperfections. The achieved precision represents the huge rejection of direct charge excitation of the cavity that results from arranging for the beam to travel through the cavity on a line for which, by left-right symmetry, there is no net cavity excitation. With no further

refinements of the S-G detection apparatus in CEBAF this might seem to leave our estimated background-error/foreground-signal ratio at about 15 to 1. This estimate has come from accepting the actually-measured ATF transverse uncertainty of 15Å as an irreducible background transverse uncertainty for the S-G detection experiment. Such a large uncertainty would be expected to make detection of a Stern-Gerlach signal less than persuasive. We are therefore left with the task of showing how the S-G-induced betatron r.m.s. amplitude error can be further reduced, preferably by at least two orders of magnitude.

2.2. Background Rejection by Polarized Beam Preparation. We are finally in a position to understand two sentences copied from the second paragraph of the abstract to the present paper: "The effect of this beam preparation is to produce a bunch repetition frequency of 0.5 GHz different from the bunch polarization frequency of 0.25 GHz. This difference will make it possible to distinguish Stern-Gerlach-induced bunch deflections from charge-induced deflections."

Figure 5 is explained in detail in a later section. For now we only note that the foreground S-G betatron signal oscillates at (harmonics of) 0.25 GHz, while the background charge signal oscillates at (harmonics of) 0.5 GHz. (The extent to which this is not entirely true is discussed later.) Ideally the S-G detector would be tuned to the 0.25 GHz fundamental. But such a cavity would be inconveniently large. Rather the S-G detector is tuned to the third harmonic at 0.75 GHz. This maximizes its foreground response and minimizes its background response.

Ordinary beam position measurement is made difficult by the fact that the spurious background oscillations occur at the same frequency as the foreground transverse signal. The only rejection of the spurious signal comes from the cavity tuning to the displacement-sensitive resonator mode frequency. The previously discussed limitation of ILC detectors to nm-scale precision reflects the difficulty of rejecting spurious signals when background and forground oscillation frequencies are the same.

With the beam preparation described in Section 4 the S-G detection is much more favorable. Approximately the same spurious signal rejection ratio as before comes from beam centering (to reject direct charge signal) and the cavity's being tuned to the position-sensitive mode frequency. But, because, the charge sensitive signal amplitude at the cavity mode frequency has already been eliminated (i.e. greatly reduced) its spurious background signals are correspondingly reduced.

The inconvenient feature that the charge sensitive mode frequency is lower than the position sensitive mode frequency remains present, however. The fact that the charge sensitive TM_{110} mode frequency is *lower* than the position sensitive TM_{210} makes it impossible to improve the selectivity by low pass filtering. This limitation can manifest itself by saturation of external detection apparatus on a spurious low frequency signal of large amplitude. This is mainly just a nuisance to be worked around, perhaps by notch filtering at the TM_{110} frequency.

The proposed improvement in S-G detection selectivity by the polarized beam preparation just described should already produce the two or three orders of magnitude

in background rejection needed to make a convincing demonstration of S-G detectability possible. To use the S-G signal for accurate determination of beam polarization may need more effective background rejection.

2.3. Stern-Gerlach Signal Extraction by Sideband Detection. There is another way to reduce the spurious background signal. It is operationally possible to modulate the two CEBAF beam polarizations independently. This modulation has the effect of shifting the S-G response signals to be sidebands of the bunch repetition frequency. (Except for the possibility of upstream beam steering correlated with the modulation) this moves the S-G signal to an externally-controllable frequency accessible to S-G oscillation but not to conventional betatron oscillation. Currently this polarization modulation capability is available for low frequencies up to several KHz, which is much higher than needed for the detection scheme to be described here.

We assume the polarization of the superimposed A and B beams are modulated with frequency ω_m. The time domain, $i\,p(t)$ current-polarization products of the separate A and B beams are given by

$$\begin{aligned} i\,p^A(t) &= \sum_{n=-\infty}^{\infty} \delta(t - nT_0)(A + a\cos\omega_m t) \\ i\,p^B(t) &= \sum_{n=-\infty}^{\infty} \delta(t - T_0/2 - nT_0)(A + a\sin\omega_m t). \end{aligned} \tag{1}$$

and are plotted on the left in Figure 2. The modulation amplitude a is necessarily smaller in magnitude than the un-modulated polarization amplitude A. There are two essential differences between the A and B beams. The more essential difference is that the beam pulses are shifted in time by one half cycle. The less essential difference is that the cosine modulation has been replaced by sine modulation. (Other polarization modulations are possible.) The modulation frequency ω_m, for which the frequency is expected to be in the range $0 < f_m < 1\,\mathrm{kHz}$, is exaggerated by many orders of magnitude in this figure, since $f_0 = 1/T_0$ is about $0.75\,\mathrm{GHz}$. Champeney[**9**] gives the A-beam, cosine-modulated current-polarization Fourier tranform $IP^A(\omega)$ to be

$$I\,P^A(t) = \sum_{n=-\infty}^{\infty} \frac{2\pi}{T_0}\left(A\delta\Big(\omega - n\frac{2\pi}{T_0}\Big) + \frac{a}{2}\,\delta\Big(\omega - n\,\frac{2\pi}{T_0} + \omega_m\Big) + \frac{a}{2}\,\delta\Big(\omega - n\,\frac{2\pi}{T_0} - \omega_m\Big)\right). \tag{2}$$

The Fourier transform of the B-beam is given by

$$\begin{aligned} &I\,P^B(t) \\ &= e^{-iT_0\omega/2} \sum_{n=-\infty}^{\infty} \frac{2\pi}{T_0}\left(A\delta\Big(\omega - n\frac{2\pi}{T_0}\Big) + i\,\frac{a}{2}\,\delta\Big(\omega - n\,\frac{2\pi}{T_0} + \omega_m\Big) + i\,\frac{a}{2}\,\delta\Big(\omega - n\,\frac{2\pi}{T_0} - \omega_m\Big)\right) \\ &= \sum_{n=-\infty}^{\infty} \frac{2\pi}{T_0}\left(A\,(-1)^n\,\delta\Big(\omega - n\frac{2\pi}{T_0}\Big) + i\,\frac{a}{2}\,\delta\Big(\omega - n\,\frac{2\pi}{T_0} + \omega_m\Big) + i\,\frac{a}{2}\,\delta\Big(\omega - n\,\frac{2\pi}{T_0} - \omega_m\Big)\right). \end{aligned} \tag{3}$$

where, having moved the time-shift factor, $e^{-iT_0\omega/2}$ inside the summation, its ω factor can be replaced by $2\pi n/T_0$, this factor multiplies a delta function with argument $\omega - 2\pi/T_0$. The corresponding time shift of the modulation is being neglected.

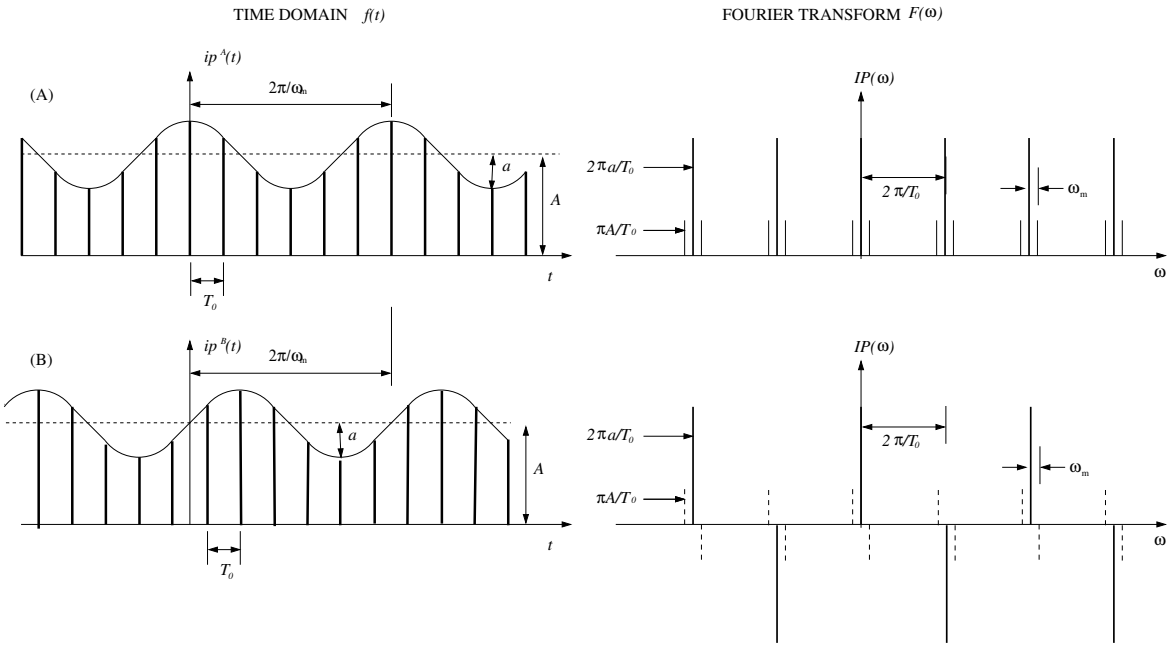

FIGURE 2. Time domain and frequency domain beam pulses for the A and B staggered, modulated-polarization beams. Broken Fourier amplitude lines indicate they are "pure imaginary", proportional to "i". In summing the A and B beam polarization signals the odd harmonics cancel and the even harmonics add, in effect cutting the polarization frequency in half. As required, all harmonics of the beam current itself add constructively, thereby conserving the beam current fundamental frequency.

A clean Stern-Gerlach will be made available by narrow frequency filtering to one or the other of the modulation sideband frequencies.

2.4. Stern-Gerlach Signal Extraction by Synchronous Detection. So far the only application of polarization modulation has depended on narrow band filtering at sideband frequencies. In fact, since these frequencies are externally imposed, there is the possibility of further noise reduction by synchronous detection that exploits previously ignored phase information.

3. Stern-Gerlach Deflection of a Relativistic Particle

We are primarily interested in the Stern-Gerlach deflection caused by the passage of a point particle with velocity $v\hat{\mathbf{z}}$ and rest frame, transversely-polarized magnetic dipole moment vector $\mu_x^*\hat{\mathbf{x}}$, through a DC quadrupole, of length L_q, that is stationary in the laboratory frame K. The purpose of this section is to relate the Stern-Gerlach

and Lorentz force deflections in a quadrupole in a transfer line such as the CEBAF injection line.

It is convenient to formulate the calculation with an (abundantly valid) impulsive approximation, in which the integrated momentum imparted to a particle passing through a quadrupole are small enough to justify neglecting the spatial displacement occurring during the encounter and keeping track of only the angular deflection. One also notes the particle speed is conserved because it is only a longitudinal component of force that can change the particle speed.

This is illustrated in Figure 3. The lower part of the figure illustrates the situation in a frame K' which is a particle rest frame applicable at the instant the center of the resonator passes the particle. Before and after momentum vectors are shown in the

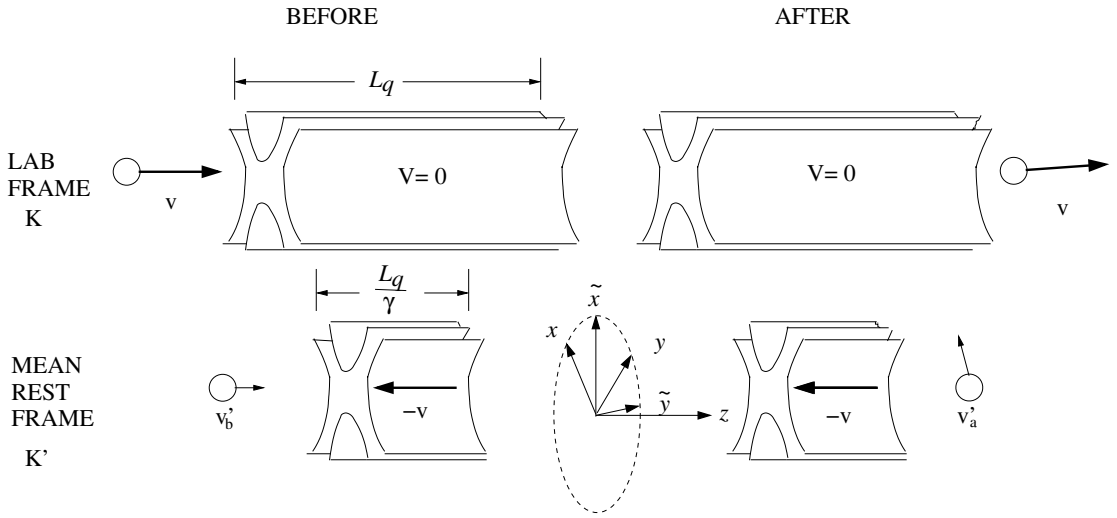

FIGURE 3. Pictorial representations of interaction between relativistic particle and quadrupole magnet, as viewed both from the laboratory frame K and from a "mean rest frame K'" (the electron rest frame at the instant the electron passes the center of the magnet). Lorentz contraction makes the moving magnet appear shorter. $v_b'\hat{\mathbf{z}}$ is the miniscule, non-relativistic, before-encounter particle velocity of the particle in the K' frame. The magnet velocity is unchanged in the encounter. The "erect" coordinate system is (x, y). The "skew" coordinate system is $(\tilde{x}, \tilde{y})$.

figure. We anticipate the small transverse Stern-Gerlach deflection shown. But there is also the possibility of longitudinal momentum transfer, from magnet to particle. For a magnet at rest (in frame K') this momentum transfer would vanish but, because the magnet is moving, there is the (controversial) possiblity of longitudinal momentum transfer. Nevertheless, this would only be an end effect, fractionally small for our, assumed-to-be-sufficiently-large, L_q. Under these assumptions the Stern-Gerlach deflection in the instantaneous rest frame can simply be copied from well-established

non-relativistic formalism[**4**]; the transverse force is given by

$$\tilde{F}'_{\tilde{x}} = \mu^*_{\tilde{x}} \frac{\partial \tilde{B}'_{\tilde{x}}}{\partial \tilde{x}'}. \tag{4}$$

All coordinates and components have been assigned overhead tildes for reasons to be justified shortly. Following notation of Conte[**5**], the rest frame magnetic moment is symbolized by μ^* to stress that it is specific to the rest frame, irrespective of whatever reference frame is being discussed. The time spent by the particle in the magnetic field is L'_q/v, and the integrated, rest frame transverse momentum impulse is

$$\widetilde{\Delta p'}_x = \tilde{F}'_{\tilde{x}} \frac{L'_q}{v} = \frac{\mu^*_{\tilde{x}}}{v} \frac{\partial}{\partial \tilde{x}'} (\tilde{B}'_{\tilde{x}} L'_q). \tag{5}$$

As viewed in the K' rest frame, the passing magnet is Lorentz-contracted to length $L_q/\gamma_{_V}$. To determine B'_x the laboratory magnetic field $\tilde{B}_{\tilde{x}}$ needs to be Lorentz transformed to the moving frame K'. This produces both an electric and a magnetic field, but it is only the magnetic field that produces Stern-Gerlach displacement in the particle's rest frame. The Lorentz transformation yields[**6**] $\tilde{B}'_{\tilde{x}} = \gamma \tilde{B}_{\tilde{x}}$. We conclude that the product $\tilde{B}_{\tilde{x}} L_q = \tilde{B}'_{\tilde{x}} L'_q$ is the same in laboratory and rest frames. Since the displacement $\tilde{x} = \tilde{x}'$ and the transverse momentum component $\widetilde{\Delta p}'_{\tilde{x}} = \widetilde{\Delta p}_{\tilde{x}}$ are also invariant for Lorentz transformation along the z axis, Eq. (5) becomes

$$\widetilde{\Delta p}^{SG}_{\tilde{x}} = \tilde{F}_{\tilde{x}} \frac{L_q}{v} = \frac{\mu^*_{\tilde{x}}}{v} L_q \frac{\partial \tilde{B}_{\tilde{x}}}{\partial \tilde{x}}. \tag{6}$$

The equation for $\widetilde{\Delta p}^{SG}_{\tilde{y}}$ is obtained by replacing $\partial \tilde{B}_{\tilde{x}}/\partial \tilde{x}$ by $\partial \tilde{B}_{\tilde{y}}/\partial \tilde{y}$. The "SG" superscripts have been introduced to distinguish Stern-Gerlach deflections from Lorentz force deflections.

The conclusion so far is that formula 4, derived initially assuming non-relativistic kinematics, is valid even for relativistic particle speed. Of course, because v cannot exceed c, the transverse force saturates as the particle becomes relativistic. Since the particle momentum continues to increase proportional to γ, the angular deflection falls as $1/\gamma$.

As indicated in Figure 3, the coordinates with tildes are actually "skew" coordinates in conventional accelerator terminology. The "erect" coordinates are (x, y) and each iron pole tip of an erect quadrupole is a hyperbola asymptotic to an x and a y axis. The magnetic field components of an erect DC quadrupole are given by

$$B_x = ky, \quad B_y = kx, \quad \text{where} \quad k = \frac{\partial B_x}{\partial y} = \frac{\partial B_y}{\partial x}, \tag{7}$$

Treating a quadrupole of length L_q as a thin lens, the Lorentz force on a point particle of mass m and charge e traveling with velocity $v\hat{\mathbf{z}}$ through the quadrupole imparts momentum

$$\Delta \mathbf{p} = \mathbf{F}(x, y)\, \Delta t = ev\hat{\mathbf{z}} \times (ky\hat{\mathbf{x}} + kx\hat{\mathbf{y}}) \frac{L_q}{v} = eL_q k(y\hat{\mathbf{y}} - x\hat{\mathbf{x}}). \tag{8}$$

The relativistic longitudinal particle momentum of the particle is $p = \gamma m v$ and its (small) angular deflections are given by

$$\Delta\theta_x \hat{\mathbf{x}} + \Delta\theta_y \hat{\mathbf{y}} = \frac{\Delta \mathbf{p}}{p} = \frac{eL_q k}{p}(-x\hat{\mathbf{x}} + y\hat{\mathbf{y}}) \equiv q_x x\hat{\mathbf{x}} + q_y y\hat{\mathbf{y}}. \tag{9}$$

The final equation *defines* inverse focal lengths $q_x = 1/f_x$ and $q_y = 1/f_y$ of the quadrupole treated as a (geometric optics) thin lens;

$$q_x = -\frac{eL_q k}{p} = -\frac{L_q c\partial B_y/\partial x}{pc/e}, \quad \text{and} \quad q_y = \frac{eL_q k}{p} = \frac{L_q c\partial B_y/\partial x}{pc/e}. \tag{10}$$

This confirms the well-known result that a quadrupole focusing in one plane is defocusing in the other. The right-most expressions are arranged for convenience of evaluation in MKS units, with pc/e expressed in volts. For the line in question $pc/e = 123\,\mathrm{MV}$.

The coordinates and magnetic components in the erect and skew frames are related by

$$x = \frac{1}{\sqrt{2}}\left(\tilde{x} - \tilde{y}\right), \quad y = \frac{1}{\sqrt{2}}\left(\tilde{x} + \tilde{y}\right), \tag{11}$$

$$B_x = \frac{1}{\sqrt{2}}\left(\tilde{B}_{\tilde{x}} - \tilde{B}_{\tilde{y}}\right), \quad B_y = \frac{1}{\sqrt{2}}\left(\tilde{B}_{\tilde{x}} + \tilde{B}_{\tilde{y}}\right). \tag{12}$$

Adding and subtracting the pair of Eqs. (11) and the pair Eqs. (12) and substitution into Eqs (7) produces

$$\tilde{B}_{\tilde{x}} = k\tilde{x}, \quad \text{and} \quad \tilde{B}_{\tilde{y}} = k\tilde{y}, \tag{13}$$

from which it follows that k is also given by

$$k = \frac{\partial \tilde{B}_{\tilde{x}}}{\partial \tilde{x}} = \frac{\partial \tilde{B}_{\tilde{y}}}{\partial \tilde{y}}. \tag{14}$$

Substituting these formulas into Eq, (6) produces

$$\widetilde{\Delta p}_{\tilde{x}}^{SG} = \frac{\mu_{\tilde{x}}^*}{v} L_q k, \quad \text{and} \quad \widetilde{\Delta p}_{\tilde{y}}^{SG} = \frac{\mu_{\tilde{x}}^*}{v} L_q k, \tag{15}$$

as the Stern-Gerlach transverse momentum impulses in the quadrupole under discussion. All that remains is to relate the Stern-Gerlach and Lorentz deflections. The Stern-Gerlach angular deflections are given by

$$\widetilde{\Delta\theta}_{\tilde{x}}^{SG} = \frac{\widetilde{\Delta p}_{\tilde{x}}^{SG}}{p} = \frac{\mu_{\tilde{x}}^* L_q k}{pv}, \quad \text{and} \quad \widetilde{\Delta\theta}_{\tilde{y}}^{SG} = \frac{\widetilde{\Delta p}_{\tilde{y}}^{SG}}{p} = \frac{\mu_{\tilde{y}}^* L_q k}{pv}. \tag{16}$$

Comparing with Eqs. (10), one sees that (except for orientation issues) the Stern-Gerlach deflection in a quadrupole is strictly proportional to the inverse focal lengths of the quadrupole;

$$\boxed{\widetilde{\Delta\theta}_{\tilde{x}}^{SG} = -\frac{\mu_x^*}{ec\beta} q_x, \quad \text{and} \quad \widetilde{\Delta\theta}_{\tilde{y}}^{SG} = \frac{\mu_y^*}{ec\beta} q_y,} \tag{17}$$

These formulas are boxed to emphasize their universal applicability to all cases of polarized beams passing through quadrupoles. For all practical cases $\beta \approx 1$. With μ_x^*

and μ_y^* differing from the Bohr magnetron μ_B only by $\sin\theta$ and $\cos\theta$ factors respectively, a convenient physical constant for the evaluation is

$$\frac{\mu_B}{ec} = \frac{0.928 \times 10^{-23}\,\mathrm{J/T}}{(1.602 \times 10^{-19}\,\mathrm{C}) \times (2.9979 \times 10^{8}\,\mathrm{m/s})} = 1.932 \times 10^{-13}\,\mathrm{m}. \tag{18}$$

Numerically, Eq. (17) yields Stern-Gerlach-induced, Courant-Snyder betatron amplitudes proportional to

$$\begin{aligned} \sqrt{\beta_x}\,\widetilde{\Delta\theta}_{\tilde{x}}^{SG} &= -(1.932 \times 10^{-13}\,\mathrm{m})\,\sqrt{\beta_x}\,q_x, \\ \sqrt{\beta_y}\,\widetilde{\Delta\theta}_{\tilde{y}}^{SG} &= (1.932 \times 10^{-13}\,\mathrm{m})\,\sqrt{\beta_y}\,q_y. \end{aligned} \tag{19}$$

The $\sqrt{\beta}$ factors have been included because the transverse displacement Δx_j at downstream location "j" caused by angular displacement $\Delta\theta_i$ at upstream location "i" is given (in either plane) by

$$\Delta_j = \sqrt{\beta_j \beta_i}\,\Delta\theta_i \sin(\psi_j - \psi_i). \tag{20}$$

where $\psi_j - \psi_i$ is the betatron phase advance from "i" to "j".

Usually the lattice β-functions have either a maximum or minimum at each quadrupole location. As a result the S-G x-excitation is dominated by the quadrupoles situated at β_x maxima, and similarly for y. Furthermore, the most favorable locations for S-G x-detection BPMs is also at β_x maxima, and similarly for y. In detail, statements like this need to be qualified by the particular polarization state of the beam, taking into account that, from the Stern-Gerlach point of view, the quadrupoles are "skew".

Irrespective of this reservation, these formulas are evaluated numerically for the CEBAF injection line in a later section. See, for example, Table 1. Superficially, of the entries in the table, the largest observable S-G y-displacements are those caused at i=L8 and observed at j=R3 or j=R7. In detail, the correct betatron phase factors have to be included and phasor sums evaluated.

It is somewhat fortuitous that, because the quadrupoles at the upstream end of the CEBAF 123 MeV line are "strong", they produce "strong" S-G angular deflections. Furthermore, because the downstream quadrupoles are "weak", the downstream beta function maxima are large, which "amplifies" the $\Delta_{x,S-G}$ and $\Delta_{y,S-G}$ displacements, but without much changing the S-G betatron amplitudes. For maximum sensitivity the S-G BPMs should be located at β-function maxima.

If the quadrupoles strengths could be adjusted arbitrarily the observability of S-G-induced betatron oscillations could be greatly enhanced. As it happens, for the particular quadrupole strengths assumed in Table 1 the horizontal (x) S-G response is not very strong. Though the S-G deflections at L7 and L9 are individually strong, because their $\Delta\psi_x$ phase separation is about π, their deflections approximately cancel. This seems more like bad luck than any kind of fundamental impediment.

There is not much scope for changing the optics without compromising the beam line performance. By changing the five L-type quadrupoles that preceed the chicane the relative heights of the first two β_x peaks can probably be changed appreciably without much de-tuning of the dispersion suppression. In this way the horizontal S-G cancellation would be largely overcome to make the horizontal S-G response comparable

with the vertical response. Also the few quadrupoles following the chicane can perhaps be altered to improve the S-G detection. Resonant BPMs in this region can provide independent confirmation of the S-G betatron amplitudes. None of these things have been investigated.

Optics far more favorable for Stern-Gerlach polarimetry could surely be developed if the injection beam line quadrupoles could be altered more-or-less freely and the beam dumped at the end of the injection line.

Any betatron oscillations launched in the injection line of course continue in the main ring. The possiblity of measuring there has not been investigated. The most favorable locations would preceed the injection linac. The S-G induced betatron oscillation amplitude would be adiabatically damped in the North Linac in proportion to square root of energy, making it harder to measure.

Deflection formulas (6) exhibit no *explicit* dependence on γ. This is only because the angular deflections are expressed in terms of quadrupole inverse focal lengths. For a given quadrupole at fixed quadrupole excitation, the inverse focal length scales as $1/\gamma$. This has the effect of "hiding" the $1/\gamma$ Stern-Gerlach dependence, which is due to the proportionality to γ of the beam stiffness.

4. CEBAF Injection Line Polarized Beam Preparation

The Stern-Gerlach BPM signal is extremely weak compared to direct beam charge BPM signal. The cleanest way to extract the S-G signal is for its frequency to differ from the frequency of the charge signal. This makes it essential to shift the S-G frequency away from the bunch repetition frequency. A resonant cavity can then serve as a filter to separate the S-G signal from the direct charge signal, based on their different frequencies. In a storage ring it would be possible to exploit the spin tune precession during circulation aroung the ring to shift the bunch polarization frequency, but this option is not available in a linac beam line.

In a linear beam line, the fact that each bunch passes an S-G sensitive BPM only once, makes it hard to arrange for the polarization of successive bunches to be different. Different polarization can, however, be imposed at the electron source by superposing staggered bunch trains having opposite (or otherwise different) polarizations. This can only be done near the electron source, either by alternating the (circular) polarization of the laser of the photo-injector, or by swinging the electron polarization at the front end of the injector line, where the electron energy is still quite low. The latter possibility has been discussed earlier. The frequency with which the bunch polarization oscillates is currently thought to be limited to, perhaps, 10 kHz, which corresponds to a insufficiently long polarization oscillation period of $T_{\rm pol} \approx 100\,\mu$s.

Far higher frequency bunch polarization modulation frequency is made possible by superposing staggered bunch trains having different polarizations. Figure 4 illustrates such a superimposed CEBAF bunch train. Bunches are labeled A in one of the two pre-superimposed bunch trains and labeled B in the other. Figure 5 shows the resulting beam charge and beam polarization frequency spectra.

In the CEBAF injection line a single bunch can, similarly, pass through the S-G resonator only once. But now adjacent A and B bunches coming in the sequence

A,B,A,B,$\cdots$, can be arranged to have arbitrarily different polarizations, for example both purely transverse, but of opposite sign. Since the bunch repetition rate is of order 1 GHz, the number of S-G resonator cycles during damping time $T_{\rm damp} \approx 10^{-5}$ s is of order 10^4.

This makes possible a huge suppression of direct charge excitation relative to S-G excitation. There are however, effects that limit the effectiveness of this suppression. There will be an r.m.s. deviation σ_{AB} between the A and B bunches. Furthermore, to the extent the S-G resonator is tipped vertically by r.m.s. angle σ_{Θ_v}, the benefit that the S-G cavity resonates in a TM mode (insensitive to passing beam charge) is defeated.

This makes possible a huge suppression of direct charge excitation relative to S-G

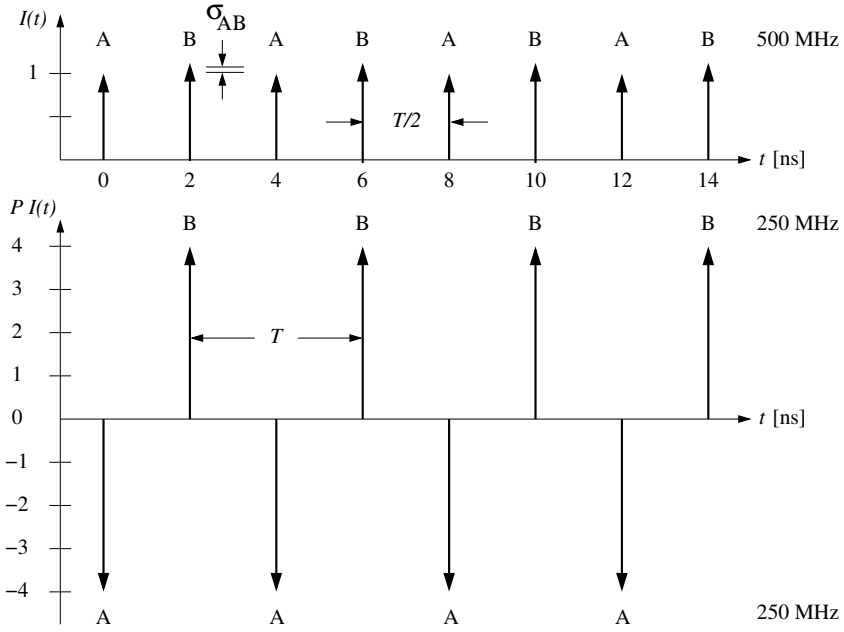

FIGURE 4. Beam A, 250 MHz, positive-polarization bunches, alternate with beam B, 250 MHz, negative-polarization bunches. (Except for σ_{AB} amplitude imbalance) the beam charge frequencies are harmonics of 0.5 GHz. i.e. 0.5, 1.0, 1.5, ... The third harmonic beam magnetization frequency is 0.75 GHz.

excitation. There are however, effects that limit the effectiveness of this suppression. There will be an r.m.s. deviation σ_{AB} between the A and B bunches. Furthermore, to the extent the S-G resonator is tipped vertically by r.m.s. angle σ_{Θ_v}, the benefit that the S-G cavity resonates in a TM mode (insensitive to passing beam charge) is defeated.

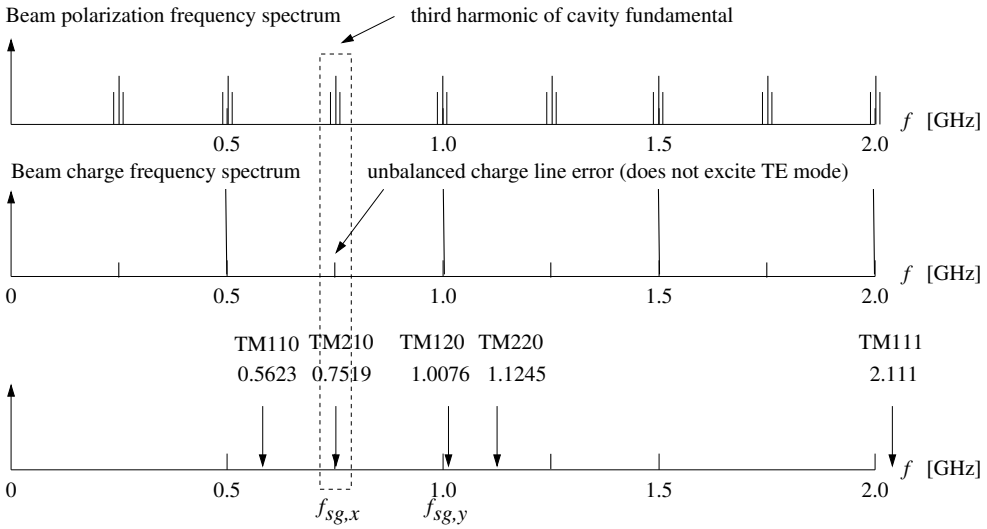

FIGURE 5. The top plot shows frequency spectra of the individual (staggered) A and B bunch currents. There is the possibility of beam magnetization side bands if the A and/or B polarizations are being modulated and $P_A I_A$ or $P_B I_B$ is plotted. The middle plot shows the frequency spectrum of the superimposed A and B bunch currents. The dominant lines are at twice the frequency of the individual currents. Mismatch of A and B currents produces background lines coinciding with magnetization lines. The bottom plot indicates the f_{S-G} frequency to which the resonator is tuned, the cut-off frequency of the fundamental, S-G sensitive TE_{10} mode, and the lowest frequency charge-sensitive TM_{11} mode.

5. Sample Determination of Stern-Gerlach Betatron Amplitudes

Table 1 provides numerical values for the main parameters of the CEBAF 123 MeV electron injection line. They have mainly been extracted by measuring and scaling from Figure 6 which corresponds to the line layout shown in Figure 7. The values are only crude and tentative for various reasons. The beamline has probably been superceeded by now, and the data extraction from the figure has been quite crude. Furthermore, when I attempt to reconstruct the optical functions from the quadrupole strengths provided in reference [**11**] I get only semi-quantitative agreement with Figure 6. As a result the $\Delta\psi$ phase advance factors in the table may be quite wrong. For these reasons the figures in this section are intended to serve as a numerical example rather than a realistic first pass design of an actual beam test.

These calculations need to be repeated starting from an up-to-date lattice description file. It will be important also to extend the lattice description at least as far as the entrance to the north area linac, and preferably around the following arc.

As explained earlier, this beamline, as it stands, is more favorable for detecting vertical S-G oscillations than horizontal. The bold face entries in the table emphasize the significant parameters in for deflecting vertical S-G deflection.

TABLE 1. Lattice optics for the CEBAF 123 MeV electron injection line. $L_q = 0.15\,\mathrm{m}$ for all quadrupoles. The bold face entries correspond to what seems like the most favorable S-G-induced betatron amplitudes for this particular adjustment of the 123 MeV injection line. The entries in the column labeled "rate-y" are $q\sqrt{\beta_i\beta_j}\,\sin(\Delta\psi_y)$.

label	s m	$\partial B_y/\partial x$ T/m	q 1/m	β_x m	$\psi_x/2\pi$	β_y m	$\psi_y/2\pi$	$\Delta\psi_y/(2\pi)$	$\sin\Delta\psi_y$	rate-y
L6	1.237	-1.403	-0.513	8.50	0.0	22.5	0.0	-0.453		
L7	3.513	3.509	1.284	65.0	0.0154	0.86	0.4135	-0.039		
L8	4.633	-3.761	**-1.376**	1.0	0.4933	**14.7**	0.4533	0	0	
L9	5.717	3.348	1.225	75.8	0.5086	3.0	0.4776	0.024	0.152	
L10	6.866	-0.848	-0.310	39.4	0.5112	3.4	0.7315	0.278	0.984	
R1	11.08	-0.117	-0.428	20.2	0.9828	3.81	0.9059	0.452	0.294	
R2	13.92	0.751	0.274	76.2	0.9907	2.54	0.9351	0.481	0.114	
R3	23.63	-0.604	-0.221	1.35	0.9982	**62.3**	1.2661	0.812	**-0.923**	**38.4**
R4	29.38	0.803	0.294	20.5	1.0004	3.90	1.3549	0.901	-0.579	
R5	34.97	-0.573	-0.210	3.3	1.4916	7.12	1.4159	0.962	-0.233	
R6	40.81	0.803	0.294	11.0	1.4981	10.2	1.4768	1.023	0.147	
R7	46.47	-0.604	-0.221	1.9	1.5003	**91.6**	1.552	1.099	**0.583**	**-29.4**
R8	56.05	0.751	0.275	75.0	1.9941	0.34	1.8897	1.436	0.390	
R9	58.92	-1.172	-0.429	18.1	1.9952	14.4	1.9227	1.469	0.191	

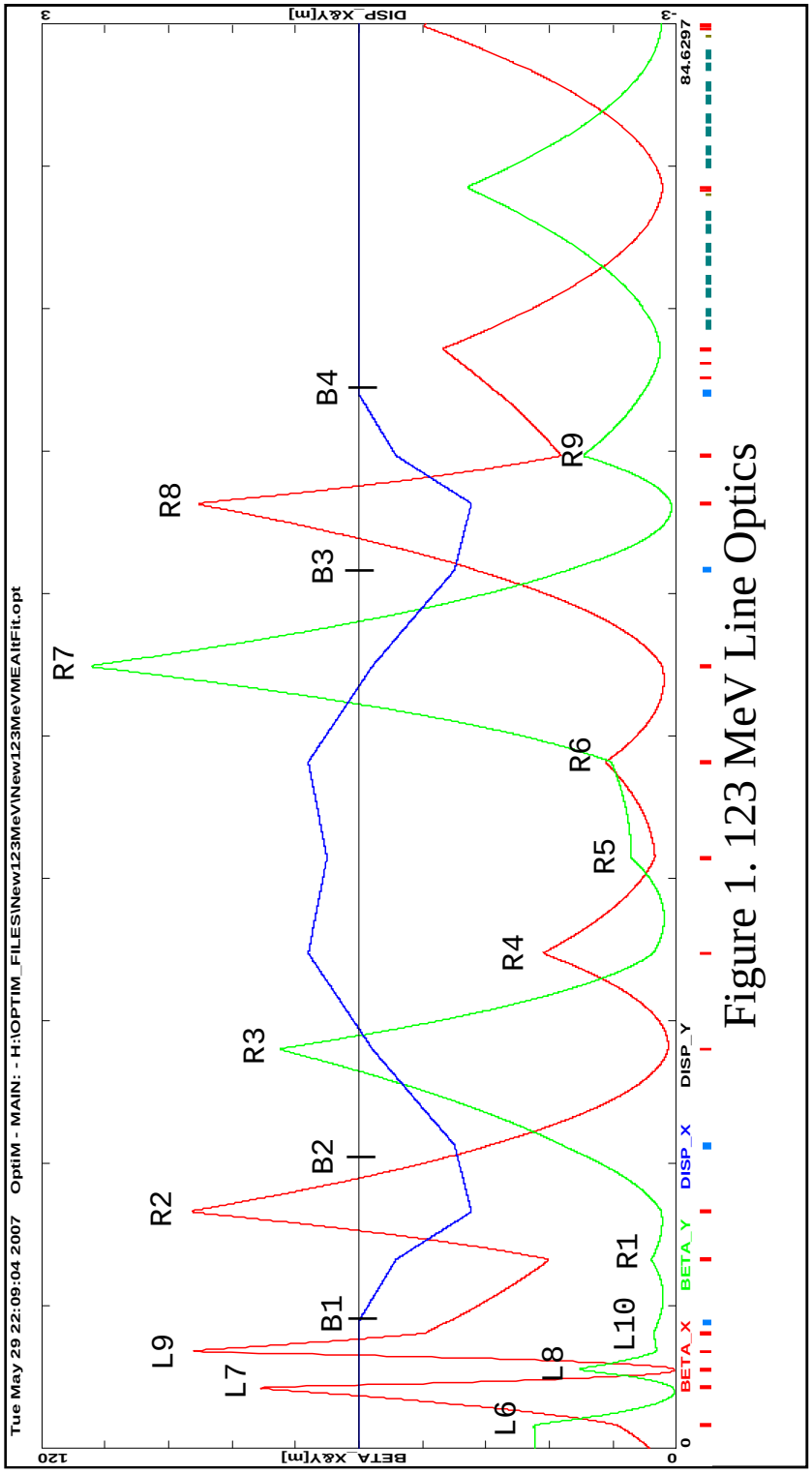

FIGURE 6. Optical functions for the 123 MeV injection line copied from reference[**11**]. This design has probable been superceded. Entries in Table 1 have been scaled from this graph.

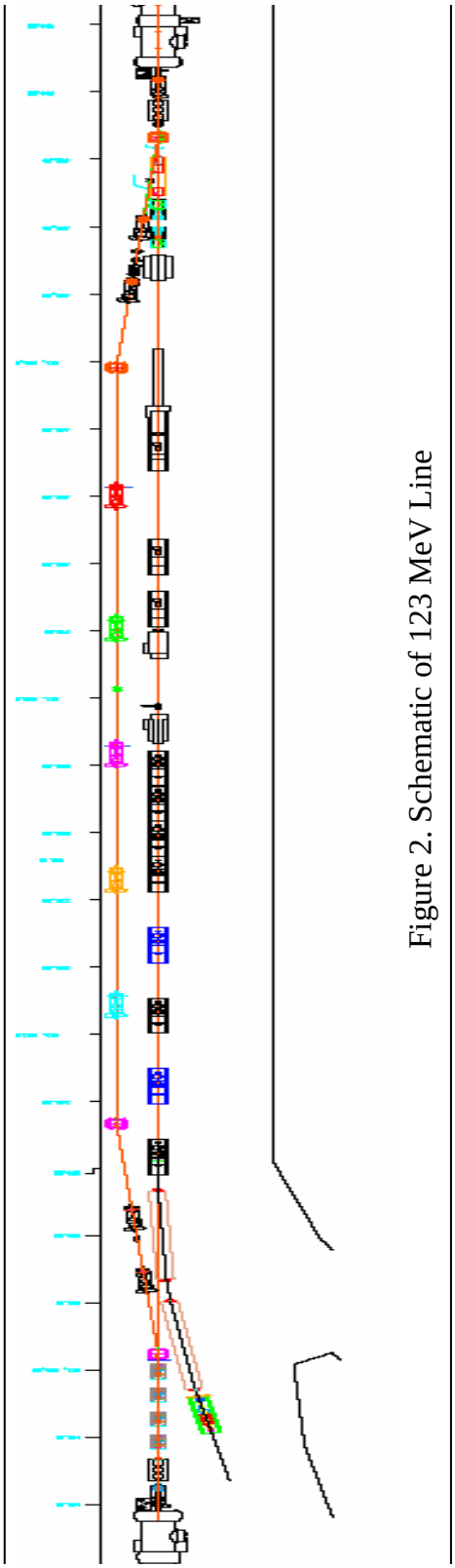

FIGURE 7. Also copied from reference[**11**], this figure gives the 123 MeV beamline layout.

Bibliography

[1] S. Walston, et al., *Performance of a high resolution cavity beam position monitor system,* Nuclear Instruments and Methods in Physics Research A, 578, p1, 2008

[2] C.J. Swinson, *Development of Beam Position Monitors for Final Focus Systems at the International Linear Collider*, Oxford University PhD Thesis, 2010

[3] N.Y. Joshi, *Design and Analysis Techniques for Cavity Beam Position Systems for Electron Accelerators,* University of London PhD Thesis, 2013

[4] J. Porter, R. Pettifer, and D. Leadly, *Direct demoonstration of the transverse Stern-Gerlach effect,* American Journal of Physics, **71**, 1103, 2003

[5] M. Conte, et al., *The Stern-Gerlach interaction between a traveling particle and a time varying magnetic field,* arXiv:physics/0003069v1 [physics.acc-ph], 2000

[6] J. Jackson, *Classical Electrodynamics,* 3rd edition, John Wiley, 1998

[7] Y. Inoue, et al., *Development of a high-resolution cavity-beam position monitor,* PRST-AB **11**, 062801, 2008

[8] Siwon Jang et al., *Development of a cavity-type beam position monitor with high resolution for ATF2,* Proceedings of IPAC2013, Shanghai, China, 2013

[9] D.C. Champeney, *Fourier Transforms and Their Physical Applications,* Academic Press, 1973

[10] S. Ramo, J. Whinnery, and T. Van Duzer *Fields and Waves in Communication Electronics,* John Wiley, p. 467-470, 1965

[11] Y. Chao et al., *123 MeVInjection Line and its Compatibility with Global Optics for 12 GeV,* JLAB-TN-07-027.